# Weak Interactions in Top-Quark Pair Production at Hadron Colliders: An Update

J.H. Kühn<sup>a</sup>, A. Scharf <sup>b</sup> and P. Uwer <sup>c</sup>

<sup>a</sup>Institut für Theoretische Teilchenphysik, Karlsruhe Institut of Technology (KIT),
76128 Karlsruhe, Germany

b Institut für Theoretische Physik und Astrophysik, Universität Würzburg,
D-97074 Würzburg, Germany

<sup>C</sup>Institut für Physik, Humboldt-Universität zu Berlin, 12489 Berlin, Germany

Weak corrections for top-quark pair production at hadron colliders are revisited. Predictions for collider energies of 8 TeV, adopted to the recent LHC run, and for 13 as well as 14 TeV, presumably relevant for the next round of LHC experiments, are presented. Kinematic regions with large momentum transfer are identified, where the corrections become large and may lead to strong distortions of differential distributions, thus mimicking anomalous top quark couplings. As a complementary case we investigate the threshold region, corresponding to configurations with small relative velocity between top and antitop quark, which is particularly sensitive to the top-quark Yukawa coupling. We demonstrate, that nontrivial upper limits on this coupling, complementary to those recently derived by the CMS and the ATLAS collaorations, are well within reach of ongoing experiments. We, furthermore, suggest a prescription that allows the implementation of these corrections in current Monte Carlo generators. Furthermore, the weak corrections are have been included in the publicly available Hathor library. The numerical results presented in this article use the same setup as the recently calculated NNLO QCD corrections. The results can thus be combined to give the most precise theoretical predictions.

#### 1. Introduction

During the past years the determination of the top quark mass, its couplings, production and decay rates has been pursued successfully at the Tevatron. Based on an integrated luminosity of almost 10 fb<sup>-1</sup> per experiment collected by both CDF and D0 at 1.96 TeV, a sample of nearly 100000 top quark pairs has been produced. The analysis of these events has led, for example, to a top mass determination of  $M_t = 173.18 \pm 0.94$ GeV [1], corresponding to a relative error of about half percent. The total production cross section  $\sigma_{t\bar{t}} = 7.65 \pm 0.42$  pb [2] determined at Tevatron is in very good agreement with the theory predictions [3–14]. The same is true for the cross section measurements performed at the LHC [15–21]. Also the  $t\bar{t}$  invariant mass distribution has been measured at LHC over a wide kinematical range [22–27]. Similar to the cross section measurements the results are in agreement with the Standard Model (SM) predictions. In contrast, surprising deviations from the theory predictions have been observed in the Tevatron experiments [28–31] by investigating the so-called charge asymmetry predicted originally fifteen years ago [32, 33]. (For discussions of theoretical predictions in the context of the SM see, for example, Refs. [34–38]).

Although these are impressive achievements already now, expectations for top quark physics at the LHC fly even higher. Based on integrated luminosities close to 5 fb<sup>-1</sup> per experiment at 7 TeV, the top mass has been determined in a combined analysis to  $M_t = 173.3 \pm 1.4$  GeV [39] already now. (Tevatron and LHC results combined have even led to a determination with an error below five permille,  $M_t = 173.34 \pm 0.76$  GeV [40].) With an integrated luminosity of more than 20 fb<sup>-1</sup> per experiment collected recently at 8 TeV, several million top-quark pairs per experiment have been produced. The high energy run at 14 TeV with its expected integrated luminosity of 100 fb<sup>-1</sup> will deliver about 10<sup>8</sup> top quark pairs per experiment during the coming years. The LHC is, obviously, a factory of top quarks, allowing for a precise determination of their properties and their production dynamics in a large kinematic region. The large center of mass energy available at the LHC will thus be used to investigate top production with partonic subenergies of several TeV and thus explore the point-like nature of the heaviest of the fundamental particles. On the theoretical side precise predictions valid at the highest accessible energies are required. With the recently completed next-to-next-to leading order OCD predictions [7–10] a major step has been taken. However when it comes to ultimate precision or highest energies weak corrections significantly affect predictions within the Standard Model. Two kinematic regions are of particular interest:

i.) Hard scattering events with partonic subenergies  $\hat{s}$  and momentum transfers  $|\hat{t}|$  and  $|\hat{u}|$  ( $\hat{s},\hat{u}$  and  $\hat{t}$  denote the partonic Mandelstam variables) far larger than  $M_t$  are affected by large negative corrections. These may reach nearly twenty percent, affecting transverse-momentum and angular distributions, and might well mimic anomalous top quark couplings. These negative corrections — if not taken into account in the theoretical predictions — could also hide a possible rise of the cross section due to a heavy resonance.

ii.) The rate for events very close to the production threshold, with relative top-antitop velocity  $\beta \le M_H/M_t$  is enhanced by the exchange of the relatively light Higgs boson. This effect can be approximately described by a Yukawa potential and is reminiscent of Sommerfeld rescattering corrections.

Weak corrections to top quark pair production have first been been studied twenty years ago [41]. The complete results, where some deficiencies were corrected and the result given in closed analytical form, can be found in Refs. [42,43] and Refs. [44,45] for quark- and gluon-induced processes, respectively. Numerical results (which, however, differed from those presented in Refs. [44, 45] and were corrected later) have been published in Ref. [46]. Purely electromagnetic corrections, which can be handled separately from the weak corrections, are evaluated in Ref. [47]. As a consequence of cancellations between the positive contributions from  $\gamma g$ -fusion and negative corrections to  $q\bar{q}$ -annihilation the combined effect amounts at most to -4%, if one considers  $p_T$ -values as high as 1.5 TeV. The impact on the  $\sqrt{\hat{s}}$  distribution remains below 1%. The details of these corrections are strongly cut-dependent and we refer to Ref. [47] for details.

In the present paper we refrain from repeating the somewhat lengthy analytical formulae for the weak corrections and concentrate on the physics implications. We also update results previously obtained using modern parton distribution functions (PDF's) and the most recent values for the input parameters. In Section 3 we present a prescription which allows the combination of electroweak and NLO QCD corrections in the framework of current Monte Carlo generators. Subsequently, in Section 4, we study the impact of enhanced Yukawa couplings on the threshold behaviour in more detail and contrast these potential measurements with recent experimental limits on the Higgs boson decay rate.

## 2. Large momentum transfers

Before entering the detailed numerical discussion, let us recall the basic qualitative aspects of weak corrections for the present case. With the Born amplitudes being of order  $\alpha_s$  (Figs. 1 a)-d) both for quark and gluon induced QCD processes, and of order  $\alpha_{\text{weak}}$  for the lowest order weak process (Fig. 1 e), weak corrections start entering the cross section at loop-induced order  $\alpha_s^2 \alpha_{\text{weak}}$  only. The absence of an interference term between the lowest order strong and neutral current amplitudes in the quark induced process, which would be of order  $\alpha_s \alpha_{\text{weak}}$ , follows trivially from the different colour flow in the two relevant amplitudes Fig. 1a and e, respectively.

Sample diagrams for weak corrections to quark- and gluon-induced amplitudes using the 't Hooft-Feynman gauge are shown in Figs. 2 and 3 ( $\phi$  and  $\chi$  denote the Goldstone bosons). For gluon fusion weak effects start as corrections to the QCD induced amplitudes.

For quark-antiquark annihilation the situation is more involved in view of a specific class of order  $\alpha_s^2 \alpha_{\text{weak}}$  contributions to the quark induced processes, which must be considered separately. In this case weak and strong interaction are intimately intertwined, and corrections

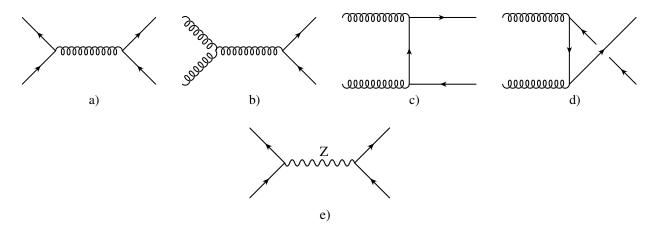


Figure 1: Lowest order QCD (a-d) and weak (e) amplitudes

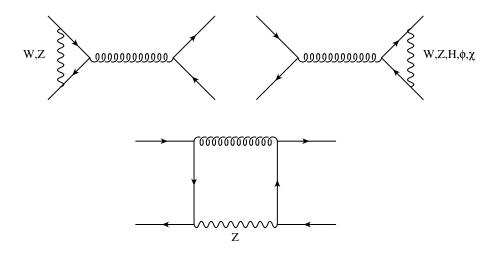


Figure 2: Sample diagrams for the virtual corrections to the quark-induced process.

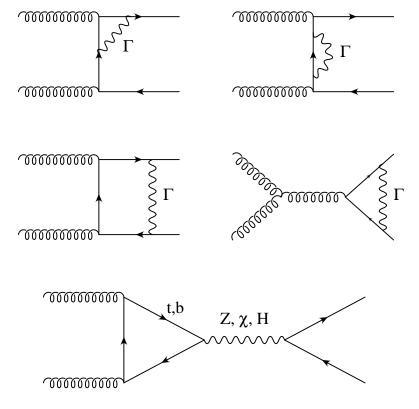


Figure 3: Sample diagrams for the virtual corrections for the gluon-induced process.  $\Gamma$  stands for all contributions from gauge boson, Goldstone boson and Higgs exchange.

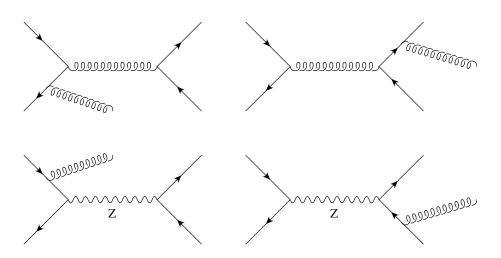


Figure 4: Sample diagrams for the real corrections to the quark-induced process.

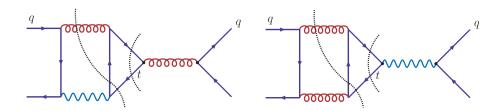


Figure 5: Sample diagrams for the proper combination of virtual and real corrections to the quark-induced process. The dotted lines show different cuts corresponding to virtual and real corrections.

with virtual and real (Fig. 4) gluon emission must be combined to arrive at an infrared finite result. The proper combination of real and virtual contributions is illustrated in Fig. 5. This issue is discussed in more detail in Ref. [42]. Only a specific combination of couplings is present in this case: The top quark triangle in Fig. 5 is attached to two gluons with vector coupling. As long as we are interested in parity-even observables (like incl. cross sections or  $p_{\rm T}$ -distributions), the light quark coupling to the Z boson is restricted to its axial coupling  $g_A^q$  proportional to its isospin  $I_3^q$ . This, in turn, leads to a strong cancellation of this specific type of correction between u- and d-quark induced processes. Since, furthermore, these contributions are small (see Fig IV.3 of Ref. [42]) for one species of quarks already, (less than one percent at threshold and about two percent at very high energies), this group of corrections will be neglected in the following discussion. This observation might, eventually, facilitate the combination of strong and weak corrections discussed at the end of this paper.

For large parton energies the total corrections are negative, for quark- as well as for gluon-induced processes. However, as a consequence of the non-vanishing weak charge both in the initial as well as in the final state, the corrections for quark induced top production are about twice those of the gluon induced process, with important consequences for the energy dependence of the corrections.

As discussed in Ref. [45] for proton-proton collisions at 14 TeV, the total cross section for top production is dominated by gluon fusion. In contrast, production of top quarks with at large transverse momenta is mainly induced by quark-antiquark annihilation, a consequence of the different parton luminosities (see Fig. 6 and 7 for LHC running at 8 TeV, results for LHC operating at 13 or 14 TeV are given in appendix A.2). The relative increase of the the quark-induced processes in combination with the different strength of the weak corrections for the two reactions thus leads to an additional increase of weak corrections for very large transverse momenta.

For the numerical results presented in this paper we use the parton distribution function MSTW2008NNLO PDF set<sup>1</sup> [48], evaluated at a factorization scale  $\mu_F = M_t$ , and the cou-

<sup>&</sup>lt;sup>1</sup>We follow closely the setup used for the NNLO QCD corrections [8–10] so that the results presented here can be directly combined.

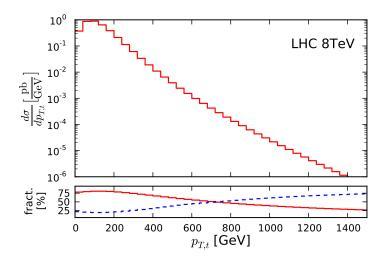


Figure 6: Leading-order differential cross section for the LHC (8 TeV) as a function of  $p_{\rm T}$ . The lower plot shows the fraction from gluon fusion (red,solid) and the fraction from quark–antiquark annihilation (blue, dashed).

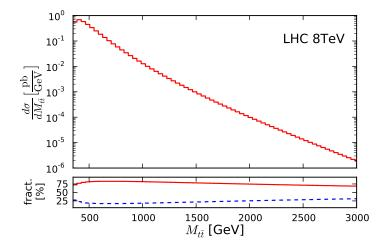


Figure 7: Leading-order differential cross section for the LHC (8 TeV) as a function of  $M_{t\bar{t}}$ . The lower plot shows the fraction from gluon fusion (red, solid) and the fraction from quark–antiquark annihilation (blue, dashed).

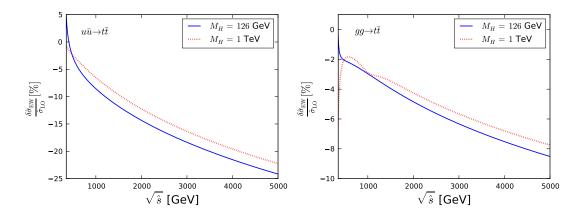


Figure 8: Relative weak corrections at parton level for the quark- and gluon-induced reactions as functions of the squared parton energy  $\hat{s}$  for two characteristic masses of the Higgs boson.

pling constants

$$\alpha(M_t) = \frac{1}{127.0}, \quad \alpha_s(M_t) = 0.106823, \quad \sin^2 \theta_W = 1 - \frac{M_W^2}{M_Z^2}.$$

For the masses we use

$$M_Z = 91.1876 \text{ GeV}, \quad M_W = 80.385 \text{ GeV}, \quad M_b = 4.82 \text{ GeV}, \quad M_t = 173.2 \text{ GeV},$$

and, if not stated otherwise,  $M_H = 126 \text{ GeV}$ .

Another important aspect is the nontrivial angular dependence of the weak corrections. As is well known, the leading Sudakov logarithms proportional  $\log^2(s/M_W^2)$  are only dependent on the (weak) charge of the incoming and outgoing particles, subleading terms may exhibit a nontrivial angular dependence (see e.g. [50,51]). This is reflected in characteristic angular dependent virtual corrections which affect the rapidity distributions of top quarks at the LHC and might well mimic anomalous couplings of the particles involved.

Let us now enter the description of the corrections in more detail. The corrections at the partonic level are shown in Fig. 8 for quark and gluon induced processes as functions of  $\hat{s}$ . For the quark—anti-quark channel we include only the infrared finite vertex corrections which are responsible for the Sudakow suppression at large momentum transfer. The box contributions for the  $q\bar{q}$  process are important only for the charge-asymmetric piece [34–38], and can be neglected in the present context. As expected, away from very small  $\hat{s}$  the corrections are negative and about twice as large for quark- compared to gluon-induced processes. Only very close to threshold one observes corrections which become positive for a light Higgs boson and will be discussed in section 3. For the ficticious case of  $M_H = 1$  TeV two pronounced structures are visible in the gluon-fusion channel: The interference between the Born amplitude and the s-channel Higgs boson contribution (last diagram of Fig.3) is visible as slight

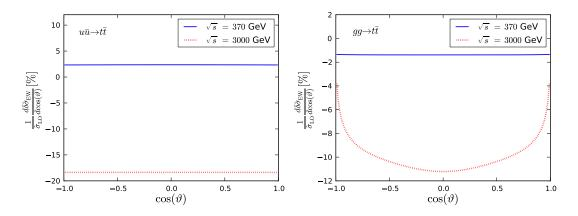


Figure 9: Relative weak corrections for the quark- and gluon-induced reactions as functions of the scattering angle close to threshold ( $\sqrt{\hat{s}} = 370 \,\text{GeV}$ , solid line) and at high energies ( $\sqrt{\hat{s}} = 3 \,\text{TeV}$ , dotted line)

depletion around 1 TeV, the interference with the Z plus  $\chi$  contribution arising from the same diagram is responsible for the dip close to threshold. For  $M_H = 126$  GeV this dip is overcompensated by the positive contribution of roughly 5% from the Yukawa interaction discussed in more detail in section 3. This same difference of 5% between  $M_H = 126$  GeV and 1 TeV is also visible in the threshold behaviour of the  $q\bar{q}$ -initiated reaction.

The angular dependence of the corrections is shown in Fig. 9 separately for quark and gluon induced processes close to threshold at 370 GeV (upper solid blue curve) and for 3 TeV (lower dotted red line). Let us, in a first step, discuss the results for the quark-induced reaction (Fig. 9 left). Again we restrict the analysis to the vertex correction. Close to threshold the process is dominated by (isotropic) S-waves, at high energies (3 TeV) the Dirac form factor dominates both for Born amplitude and correction. This leads to a constant ratio as function of the scattering angle. At low energies ( $\sqrt{\hat{s}} = 370 \text{ GeV}$ ) we find a positive correction of about 2 %. At large energies, say  $\sqrt{\hat{s}} = 3\text{TeV}$ , the Sudakow suppression leads to negative corrections of about -18%. Note that the box diagrams while not particularly enhanced would lead to sizable asymmetric and small symmetric corrections. For details we refer to Ref. [36]. The gluon induced part, in contrast, is markedly angular dependent. For large  $\hat{s}$  and small scattering angle the corrections are small, since the Sudakov-like behaviour cannot be expected in this case. At ninety degrees, in contrast, the Sudakov limit is applicable and the corrections become large. Let us now discuss observables at the hadron level. In difference to the discussion at parton level we include in the analysis now also box-contributions and real corrections, thus the full set of corrections are investigated. The corrections for the total cross section are shown in Fig. 10 as function of  $\sqrt{s}$ , for two characteristic choices of the Higgs mass,  $M_H = 126 \text{ GeV}$ and 1000 GeV. We allow  $M_H$  to move away from its recently determined value to illustrate the effect of the Higgs-top Yukawa coupling. The corrections are evidently small, of order minus two percent for all LHC energies and only moderately sensitive to  $M_H$ . Given the recent progress concerning the NNLO QCD calculations the theoretical uncertainties will eventually

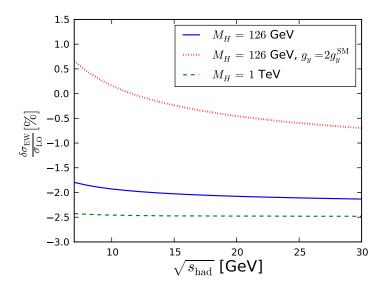


Figure 10: Relative weak corrections for the total cross section as functions of the total cms energy for two different masses of the Higgs boson and for a rescaled Yukawa coupling.

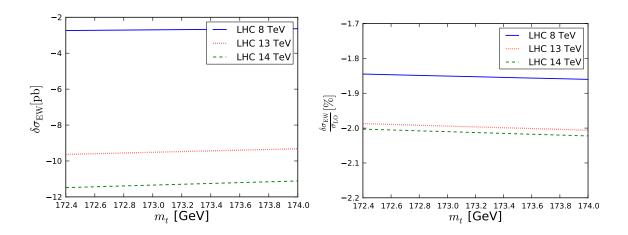


Figure 11: Weak corrections as function of the top-quark mass.

reach 3-4%. At this level of accuracy the weak corrections become important and need to be taken into account. As reference we show in Fig. 11 the weak correction as function of the top-quark mass. At 8 TeV centre of mass energy the corrections are about -1.85%. At 14 TeV the high-energy regime of the cross section becomes more accessible leading to slightly larger corrections of the order of -2.0%. For convenience we provide a parametrisation for the weak corrections valid for  $172.4 < M_t < 174$ :

$$\delta \sigma_{\text{EW}}^{8\text{TeV}} = -2.69 \text{pb} + 0.06 \text{pb} \times (M_t/\text{GeV} - 173.2)$$
 (1)

$$\delta \sigma_{\text{EW}}^{13\text{TeV}} = -9.48\text{pb} + 0.20\text{pb} \times (M_t/\text{GeV} - 173.2)$$
 (2)

$$\delta\sigma_{EW}^{8\text{TeV}} = -2.69\text{pb} + 0.06\text{pb} \times (M_t/\text{GeV} - 173.2)$$
(1)  

$$\delta\sigma_{EW}^{13\text{TeV}} = -9.48\text{pb} + 0.20\text{pb} \times (M_t/\text{GeV} - 173.2)$$
(2)  

$$\delta\sigma_{EW}^{14\text{TeV}} = -11.30\text{pb} + 0.23\text{pb} \times (M_t/\text{GeV} - 173.2)$$
(3)

As can be seen from Fig. 11 and the parametrization above, the mass dependence is very small in the range 172.4 – 174 GeV and can be neglected for most phenomenological applications. The aforementioned results can be directly combined with NNLO results calculated using the MSTW2008NNLO PDF set [48]. Since ratios are more robust with respect to different choices for the parton distribution functions we also present a parametrization for the relative corrections:

$$\frac{\delta \sigma_{\text{EW}}^{\text{8TeV}}}{\sigma_{\text{LO}}} = -1.85\% - 0.01\% \times (M_t/\text{GeV} - 173.2),\tag{4}$$

$$\frac{\delta \sigma_{\text{EW}}^{8\text{TeV}}}{\sigma_{\text{LO}}} = -1.85\% - 0.01\% \times (M_t/\text{GeV} - 173.2),$$

$$\frac{\delta \sigma_{\text{EW}}^{13\text{TeV}}}{\sigma_{\text{LO}}} = -2.00\% - 0.01\% \times (M_t/\text{GeV} - 173.2),$$

$$\frac{\delta \sigma_{\text{EW}}^{14\text{TeV}}}{\sigma_{\text{LO}}} = -2.01\% - 0.01\% \times (M_t/\text{GeV} - 173.2).$$
(6)

$$\frac{\delta \sigma_{\rm EW}^{14\text{TeV}}}{\sigma_{\rm LO}} = -2.01\% - 0.01\% \times (M_t/\text{GeV} - 173.2). \tag{6}$$

Note that the coupling constants of the strong interactions cancels in the ratios. In addition, for the ratios the mass dependence is further reduced and completely neglible in the range 172.4 - 174 GeV. One may argue that some contributions of the QCD corrections are universal and will also correct the weak contributions (see also the discussion in section 3). Based on this assumption one may use

$$\delta \sigma_{\text{EW}} = \frac{\delta \sigma_{\text{EW}}}{\sigma_{\text{LO}}} \times \sigma_{\text{NNLO}}^{\text{QCD}} \tag{7}$$

to estimate the size of the weak corrections. For  $M_t = 173.2$  GeV this leads to

$$\delta \sigma_{\rm EW}^{\rm 8TeV} = -4.4 {\rm pb}, \tag{8}$$

$$\delta\sigma_{EW}^{8\text{TeV}} = -4.4\text{pb},$$
 (8)  
 $\delta\sigma_{EW}^{13\text{TeV}} = -15.8\text{pb},$  (9)  
 $\delta\sigma_{EW}^{14\text{TeV}} = -18.8\text{pb}.$  (10)

$$\delta \sigma_{EW}^{14\text{TeV}} = -18.8 \text{pb.}$$
 (10)

In addition we demonstrate in Fig. 10 the impact of an enhanced Yukawa coupling with  $g_Y = 2g_Y^{SM}$ . In this case the negative corrections from the large transverse momentum region are overcompensated by the positive ones for small  $t\bar{t}$  masses. Let us emphasize that such an analysis might well lead to a non-trivial limit on the top quark Yukawa coupling  $g_Y$ . The weak corrections have a trivial dependence on the Yukawa coupling. A large fraction of the corrections does not depend on  $g_{Y}$ . The production of an intermediate s-channel Higgs boson

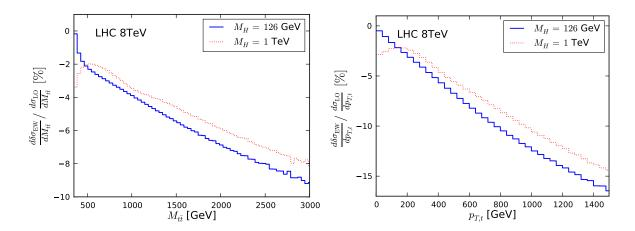


Figure 12: Relative weak corrections for the invariant  $t\bar{t}$  mass (left) and transverse momentum (right) distribution for LHC for Higgs masses of 126 GeV and 1 TeV.

through a closed b-quark loop leads to a contribution linear in the top-quark Yukawa coupling. Due to the small b-quark mass, this contribution is expected to be very small. The remaining dependence on the top-quark Yukawa coupling is quadratic, since it allways involves two  $Ht\bar{t}$ vertices. For the total cross section we find the following parametric dependence ( $M_t = 173.2$ GeV):

$$\delta\sigma_{\text{EW}}^{8\text{TeV}} = (-3.80 + 0.0009g_Y + 1.12g_Y^2)\text{pb}, \tag{11}$$

$$\delta\sigma_{\text{EW}}^{13\text{TeV}} = (-12.47 + 0.0136g_Y + 2.99g_Y^2)\text{pb}, \tag{12}$$

$$\delta\sigma_{\text{EW}}^{14\text{TeV}} = (-14.74 + 0.0146g_Y + 3.45g_Y^2)\text{pb}. \tag{13}$$

$$\delta\sigma_{\text{EW}}^{13\text{TeV}} = (-12.47 + 0.0136g_Y + 2.99g_Y^2)\text{pb}, \tag{12}$$

$$\delta\sigma_{\text{EW}}^{14\text{TeV}} = (-14.74 + 0.0146g_Y + 3.45g_Y^2)\text{pb.}$$
 (13)

Indeed we observe that the linear dependence on  $g_Y$  is very weak and can be neglected as anticipated above. Again it might be useful to study the size of the relative corrections:

$$\frac{\delta \sigma_{\text{EW}}^{8\text{TeV}}}{\sigma_{\text{LO}}} = (-2.62 + 0.0006g_Y + 0.77g_Y^2)\%, \tag{14}$$

$$\frac{\delta \sigma_{\text{EW}}^{8\text{TeV}}}{\sigma_{\text{LO}}} = (-2.62 + 0.0006g_Y + 0.77g_Y^2)\%, \tag{14}$$

$$\frac{\delta \sigma_{\text{EW}}^{13\text{TeV}}}{\sigma_{\text{LO}}} = (-2.63 + 0.0029g_Y + 0.63g_Y^2)\%, \tag{15}$$

$$\frac{\delta \sigma_{\text{EW}}^{14\text{TeV}}}{\sigma_{\text{LO}}} = (-2.63 + 0.0026g_Y + 0.61g_Y^2)\%. \tag{16}$$

$$\frac{\delta\sigma_{\rm EW}^{14{\rm TeV}}}{\sigma_{\rm LO}} = (-2.63 + 0.0026g_Y + 0.61g_Y^2)\%. \tag{16}$$

A shift of  $g_Y$  by a factor three would enhance the cross section by about 5% and might thus become experimentally accessible. As discussed in section 4, this limit can be further improved by restricting the sample to events close to the production threshold.

While for the total cross section the weak corrections are small, the situation is drastically different, once we consider differential distributions in the region of large transverse momenta  $p_{\rm T}$  or large masses  $M_{t\bar{t}}$  of the  $t\bar{t}$  system where Sudakov logarithms start to play an important role. The corrections are shown in Fig. 12 for proton-proton collisions with center of mass

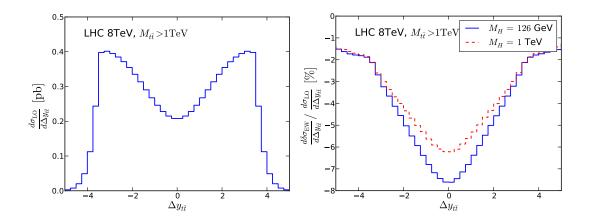


Figure 13: Rapidity distributions with invariant mass cuts at leading order (left) and relative weak corrections (right)

energies of 8 TeV and 14 TeV both for the  $p_{\rm T}$ - and the  $M_{t\bar{t}}$ -distributions. (Results for 13 and 14 TeV are shown in the Appendix.) For illustration we present again the relative corrections for Higgs masses of 126 GeV and 1 TeV. The strong increase with increasing  $p_{\rm T}$  is evident. Based on the present data sample, corresponding to to more than 20 fb<sup>-1</sup>, corrections close to -10% could be observed at  $\sqrt{s} = 8$  TeV if events with top quarks of large transverse momenta, say 750 GeV, are considered.

To investigate the angular dependence of the  $t\bar{t}$  system in its center of mass frame one could consider the distribution in the rapidity difference  $\Delta y_{t\bar{t}} = y_t - y_{\bar{t}}$  which, for fixed  $M_{t\bar{t}}$  can be directly translated into the angular distribution. To illustrate the distributions and the size of the corrections, the differential distributions  $d\sigma/d\Delta y_{t\bar{t}}$  are shown in Fig.13 for 8 TeV, considering only events with  $M_{t\bar{t}}$  larger than 1 TeV. (For 13 and 14 TeV the results are shown in the Appendix.) The corresponding relative corrections are also displayed in Fig.13. The pronounced peaking of the cross section for large rapidity differences in Fig.13 (left) is an obvious consequence of the t-channel singularity, the enhanced negative corrections around  $\Delta y_{t\bar{t}} = 0$  in Fig.13 (right) are a consequence of the Sudakov condition  $\hat{s}$  and  $|\hat{t}| \gg M_W^2$ . Since the distribution in  $\Delta y_{t\bar{t}}$  is at the same time sensitive to anomalous couplings, these could well be masked by the large radiative corrections.

#### 3. QCD and electroweak corrections combined

Let us at this point speculate about the combination of weak and QCD corrections. Clearly, the evaluation of corrections of  $O(\alpha_s \alpha)$  is out of reach in the foreseeable future. Thus, strictly speaking, both a multiplicative (of the form  $(1 + \delta_{QCD})(1 + \delta_W)$ ) and an additive (of the form  $(1 + \delta_{QCD} + \delta_W)$ ) treatment is equally justified. The difference between the two assumptions can be considered as an estimate of the theory uncertainty. It may be usefull, however, to

devise a strategy to implement eventually the major part of the combined corrections. As mentioned in the beginning, QED and purely weak corrections can be treated seperately in the present case. Furthermore, QED corrections are small and the resulting uncertainty of combined QCD and QED terms even smaller. In principle, by adjusting color coefficients, the recently available two-loop QCD corrections [8–10] could be employed to arrive at the full combined QED and QCD results. Concerning the weak corrections, we observe that a major part of the QCD corrections originates from configurations involving soft and/or collinear emission. Let us then reconstruct the effective two-body kinematics by using the  $t\bar{t}$  invariant mass as  $\hat{s}$  and the scattering angle with respect to the beam direction, as defined in the  $t\bar{t}$  rest frame as partonic scattering angle. Using this information would allow to apply the weak correction factor which also depends on  $\hat{s}$  and  $\hat{t}$  only.

Let us describe the prescriptions in more detail. As discussed before, the corrections depicted in Figs.4 and 5 can be ignored. Three overall correction factors  $K_{u\bar{u}}$ ,  $K_{d\bar{d}}$  and  $K_{gg}$  with

$$K_{ij} = \frac{d\sigma_{ij}^{\text{EW}}/d\cos(\theta)}{d\sigma_{ij}^{\text{LO}}/d\cos(\theta)}$$

remain, which are for given  $M_H$ ,  $M_W$  and  $M_Z$  functions of  $\hat{s}$  and  $\hat{t}$  and are appropriate for the three basic two-to-two processes. Numerical results for the  $K_{u\bar{u}}$  and  $K_{gg}$  are shown in Fig. 9 with  $\sqrt{\hat{s}}$  fixed to 370, and 3000 GeV. We have implemented the corresponding analytic formulae in the publicly available Hathor program [4,54] version 2.1 which is available at http://www.physik.hu-berlin.de/pep/tools/hathor.html. The correction factors for u and d quarks are nearly the same and angular independent, the correction factor for the gluon-induced process is most pronounced for top quarks produced in the transverse direction.

It is important to keep in mind that the corrections do not affect the two-to-two kinematics. This allows to implement the electroweak corrections into any Monte Carlo generator for  $t\bar{t}$  production as follows: In a first step we consider a generator which does not involve NLO QCD corrections. The invariant mass of the  $t\bar{t}$  system will be identified with  $\sqrt{\hat{s}}$ . Let us now denote the directions of the momenta of top and antitop quark in the  $t\bar{t}$  rest frame by  $\vec{e}_t^*$  and  $\vec{e}_t^*$ , respectively, the directions of the beam momenta by  $\vec{e}_1^*$  and  $\vec{e}_2^*$ , the direction of the effective scattering axis by<sup>2</sup>

$$\hat{\vec{\mathbf{e}}}^* \equiv \frac{\vec{\mathbf{e}}_1^* - \vec{\mathbf{e}}_2^*}{|\vec{\mathbf{e}}_1^* - \vec{\mathbf{e}}_2^*|} \tag{17}$$

and the effective scattering angle by

$$\cos \theta^* \equiv \vec{\mathbf{e}}_{\mathbf{t}}^* \cdot \hat{\vec{\mathbf{e}}}^*. \tag{18}$$

The partonic variables are thus obtained from

$$\hat{s} \equiv M_{t\bar{t}}^2, \ \hat{t} \equiv m_t^2 - \frac{\hat{s}}{2} (1 - \sqrt{1 - \frac{4m_t^2}{\hat{s}}} \cos \theta^*). \tag{19}$$

<sup>&</sup>lt;sup>2</sup>This approach follows the one introduced in Ref. [55] for gauge-boson pair production.

Inspecting the event, as generated through the program, more closely, it can be assigned in a unique way to the  $u\bar{u}$ ,  $d\bar{d}$  or gg induced subprocess. Using the correction functions  $K_i(\hat{s},\hat{t})$  with  $i = u\bar{u}$ ,  $d\bar{d}$  or gg, the reweighting can be performed in a straightforward way.

The kinematic prescription outlined above can also be applied to generators which include NLO QCD corrections. Events which involve collinear or soft quark or gluon emission are responsible for the major part of QCD corrections. For these events one would expect that the dominant weak corrections can still be derived from the same correction functions with  $\hat{s}$  and  $\hat{t}$  as derived from eq. (19) above. For final states with the  $t\bar{t}$  system produced at large transverse momentum, balanced by a hard quark or gluon jet at large  $P_t$ , our prescription will no longer properly account for the electroweak corrections. However, the missing terms are of order  $\alpha_s \alpha_{weak}$  and their evaluation would require the electroweak corrections for the full set of two-to-three reactions.

It remains to assign the proper correction function  $K_i$  for the full set of partonic processes. For the subprocesses  $q\bar{q}\to t\bar{t}(g)$  and  $gg\to t\bar{t}(g)$  the functions  $K_{q\bar{q}}$  and  $K_{gg}$  will be employed. The assignment of correction factors to the reaction  $qg\to t\bar{t}q$  (and its charge conjugate) is more involved. Let us assume that the incoming quark originates from hadron 1 and splits into a nearly collinear quark and gluon. The latter fuses with the gluon from hadron 2 into  $t\bar{t}$ . In this case the factor  $K_{gg}$  is suggested. Alternatively one may consider a situation where the incoming gluon splits into a nearly collinear  $q\bar{q}$  pair, with the anti-quark annihilating into  $t\bar{t}$ . In this case the use of  $K_{q\bar{q}}$  seems more adequate.

To distinguish the two options, we consider the scattering angle  $\theta_q$  of the outgoing quark relative to hadron 1 in the  $t\bar{t}$  rest frame. If  $0 \le \theta_q < \pi/2$ , we take  $K_{gg}$ , if  $\pi/2 \le \theta_q < \pi$ , we take  $K_{q\bar{q}}$ . In the limiting cases of nearly collinear emission this convention leads to the desired result, in the case of events with a quark jet at large transverse momentum the expected error will be of order  $\alpha_s \alpha_{weak}$ .

An alternative method to define a reduced kinematic in case of additional emission could be using a boost similar to what has been done in the matrix element method. The sensitivity to the specific prescription could be estimated by comparing the two different approaches.

## 4. The top-pair threshold region and the Yukawa coupling

As illustrated in Fig. 8, the corrections for top-pair production very close to threshold exhibit a significant dependence on the mass of the Higgs boson. In fact, both for quark and gluon induced process the difference in the correction between a light ( $M_H = 126 \text{ GeV}$ ) and a heavy ( $M_H = 1000 \text{ GeV}$ ) Higgs boson amounts to about 5%. This effect has been discussed in some detail for pair production at an electron-positron collider [57–61] and for quark-antiquark collisions [61] and is closely related to the well-known Sommerfeld rescattering corrections, originally obtained in the framework of QED. Similar considerations are also applicable to gluon fusion [45].

For a Yukawa potential induced by the Higgs exchange,

$$V_Y(r) = -\kappa \frac{1}{r} e^{-r/r_Y} \text{ with } \kappa = \frac{g_Y^2}{4\pi} = \frac{\sqrt{2}G_F M_t^2}{4\pi} \approx 0.0337 \text{ and } r_Y = 1/M_H,$$
 (20)

the dominant correction evaluated directly at threshold is given by the factor  $1 + \kappa \frac{M_t}{M_H}$ . (The full result including the energy dependence, can be found in [57,60].) Indeed the difference of 5% between the heavy and the light Higgs boson is well consistent with this simple approximation. For quark-antiquark annihilation the positive offset is shown in Fig.8 (left). For gluon fusion the Yukawa enhancement is partially masked by a negative contribution originating from the interference of the tree-level amplitude with the amplitude from the triangle diagrams with Z and  $\chi$  in the s-channel (Fig. 3). The difference, however, between a heavy and a light Higgs boson of about 5% remains unchanged.

As evident from Fig.8, the Yukawa enhancement is located in the region close to threshold, with relative  $t\bar{t}$ -velocity  $\beta$  less than  $M_H/M_t$ . For the moment we consider the weak corrections as an overall  $\beta$ -dependent factor which multiplies the complicated threshold behaviour induced by the partly attractive, partly repulsive QCD potential. (For QCD effects see e.g. [56] and references therein.) In principle the effect of a light Higgs exchange could be split into a short range piece, which leads to a  $\beta$ -independent correction term, and a long-range piece, which can be absorbed by adding Yukawa and QCD potential. The energy dependence can then be obtained from a Green's function treatment. This approach has been discussed in more detail in [61] for the cases of top production in electron-positron and quark-antiquark annihilation. Since  $r_Y$ , the characteristic length of the Yukawa potential, is still significantly smaller than  $r_B$ , the Bohr radius of the would-be toponium ground state,

$$r_Y/r_B = (\frac{4}{3}\alpha_s \frac{M_t}{2})/M_H \approx 1/6,$$
 (21)

the simple multiplicative treatment advocated above is sufficient for the presently required level of precision.

As discussed above, the impact on the total cross section from the variation of  $M_H$  is relatively small, less than one percent, both for the Tevatron and the LHC, and even an enhancement of the Yukawa coupling by a factor two will be hardly visible. Differential distributions, however, are significantly more sensitive to the Yukawa coupling. This is demonstrated in Figs. 14, 15, where the correction factors for the distribution with respect to  $M_{t\bar{t}}$  are evaluated for the LHC at 8 TeV and Tevatron in the region close to threshold. (Results for 13 and 14 TeV are given in the Appendix.)

As expected from the previous discussion, differences around 5% between the cases  $M_H = 126$  GeV and 1 TeV are visible. It remains to be seen, whether the experimental mass resolution and normalization of the cross section will be sufficiently precise to pin down the 5%-effect and thus determine directly the Yukawa coupling  $g_Y$ . At the same time this approach requires a detailed theoretical understanding of the QCD predictions for the threshold behaviour, governed by the remnants of the bound states, as discussed in [56]. However, in any

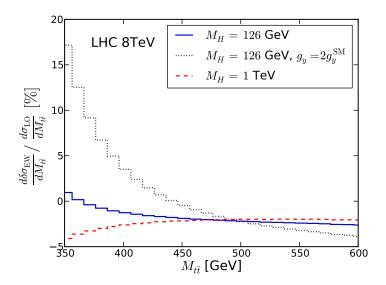


Figure 14: Relative weak corrections for the mass distribution in the framework of the SM assuming  $M_H = 126$  GeV (solid blue curve) and 1000 GeV (dashed red curve), and for the case of an enhanced Yukawa coupling  $g_Y = 2g_Y^{SM}$  with  $M_H = 126$  GeV (dotted black curve).

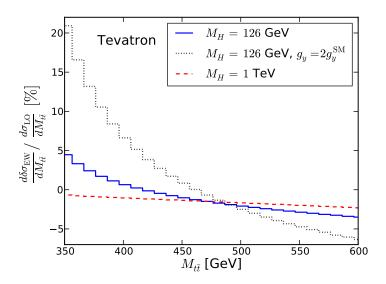


Figure 15: Same as Fig.14 but for the Tevatron.

case this approach should allow to provide an upper limit on modifications of  $g_Y$  that might be postulated in theories beyond the Standard Model <sup>3</sup>

Let us assume, for example, the case of an enhanced Yukawa coupling  $g_Y = 2g_Y^{SM}$ . This magnifies the Yukawa correction by a factor four and implies an enhancement of the cross section close to threshold by about 20%. (See dashed curves in Figs. 14, 15. Such an energy dependent offset relative to the SM prediction should be visible in Tevatron or LHC analyses. To ellaborate on this point further it is again useful to study the parametric dependence of the threshold cross section with respect to  $g_Y$  similar to what has been done in section 2 for the inclusive cross section. Restricting the cross section to the threshold region by introducing a cut on the invariant mass of the top-quark pair we find for the LHC:

$$\delta \sigma_{\text{EW}}^{8\text{TeV}}(m_{t\bar{t}} < 2M_t + 50\text{GeV}) = (-0.10 + 0.09g_Y^2)\text{pb},$$
 (22)

$$\delta\sigma_{\text{EW}}^{\text{8TeV}}(m_{t\bar{t}} < 2M_t + 100\text{GeV}) = (-0.19 + 0.13g_Y^2)\text{pb}, \tag{23}$$

$$\delta\sigma_{\text{EW}}^{\text{8TeV}}(m_{t\bar{t}} < 2M_t + 100\text{GeV}) = (-0.19 + 0.13g_Y^2)\text{pb},$$
(23)  
$$\delta\sigma_{\text{EW}}^{\text{8TeV}}(m_{t\bar{t}} < 2M_t + 150\text{GeV}) = (-0.24 + 0.13g_Y^2)\text{pb}.$$
(24)

Note that we neglected the tiny contribution linear in  $g_Y$  since it is irrelevant for the phenomenology. For the relative corrections we find:

$$\frac{\delta \sigma_{\text{EW}}^{8\text{TeV}}}{\sigma_{\text{LO}}} (m_{t\bar{t}} < 2M_t + 50\text{GeV}) = (-3.53 + 3.14g_Y^2)\%, \tag{25}$$

$$\frac{\delta \sigma_{\text{EW}}^{8\text{TeV}}}{\sigma_{\text{LO}}} (m_{t\bar{t}} < 2M_t + 50\text{GeV}) = (-3.53 + 3.14g_Y^2)\%, \tag{25}$$

$$\frac{\delta \sigma_{\text{EW}}^{8\text{TeV}}}{\sigma_{\text{LO}}} (m_{t\bar{t}} < 2M_t + 100\text{GeV}) = (-3.05 + 2.05g_Y^2)\%, \tag{26}$$

$$\frac{\delta \sigma_{\text{EW}}^{8\text{TeV}}}{\sigma_{\text{LO}}} (m_{t\bar{t}} < 2M_t + 150\text{GeV}) = (-2.83 + 1.54g_Y^2)\%. \tag{27}$$

$$\frac{\delta \sigma_{\text{EW}}^{\text{8TeV}}}{\sigma_{\text{LO}}} (m_{t\bar{t}} < 2M_t + 150 \text{GeV}) = (-2.83 + 1.54 g_Y^2)\%. \tag{27}$$

Results for 13 and 14 TeV collider energy are given in section A.1. Using  $m_{t\bar{t}} < 2M_t + 50 \text{GeV}$ we see, that doubling the Yukawa coupling would lead to a change of the cross section of about 9%. As expected, restricting the cross section to the threshold region significantly enhances the sensitivity to the top-quark Yukawa coupling. Assuming an experimental precision of 5% the top-quark Yukawa coupling can be constrained. The relevance of such a limit on  $g_Y$  can be illustrated by comparing with the limits on the Higgs couplings as suggested in Refs. [64,65] and presented recently by both CMS [66] and ATLAS [67] collaborations. In these papers it has been demonstrated that a universal rescaling  $g^{SM} \rightarrow \kappa g^{SM}$  combined with an increase of the Higgs width by a factor  $\kappa^4$  (e.g. through some presently invisible mode) can be excluded for values of  $\kappa^4$  exceeding 7.7 [67] or even 5.4 [66]. Such a rescaling would also involve the top quark Yukawa coupling, and it remains to be seen, if similar limits can be obtained from analysis of the top quark threshold behaviour.

<sup>&</sup>lt;sup>3</sup>For examples where this has been discussed in the framework of a two-Higgs-doublet model see e.g. Refs. [62, 63]

#### 5. Outlook and conclusions

A sizable data sample has been collected by LHC experiments at a center-of-mass energy of 8 TeV, and the Higgs boson has been discovered with a mass of about 126 GeV. In view of these developments an update of the weak corrections to top quark pair production has been presented. We demonstrate that these corrections start to become important already for the 8 TeV run, if an experimental precision of 5 percent can be reached. This observation applies both for large transverse momenta, say above 500 GeV, where negative corrections around 5% are observed, and for top quark production close to threshold which is enhanced by about 5% due to the attractive Yukawa interaction. A detailed study of the top-antitop spectrum close to threshold could, therefore, determine the strength of the Yukawa coupling or, at least provide interesting upper limits. We also investigate the distribution of top and antitop with respect to their rapidity difference  $\Delta y_{t\bar{t}}$  for the subsample with large invariant mass and observe marked distortions of order 8% (LHC8) and 12% (LHC14). Clearly these effects might be misinterpreted as evidence for anomalous couplings and thus have to be well under control. Last not least we indicate a possible approach for combining QCD and weak corrections in the framework of a Monte Carlo generator.

#### Acknowledgments

The work of J.H.K. was supported by BMBF Project 05H12VKE. Discussions with Jeannine Wagner-Kuhr on experimental issues are gratefully acknowledged. The work of P.U. was supported by BMBF Project 05H12KHE. The work of A.S. has been partly supported by the German Ministry of Education and Research (BMBF) under contract no. 05H12WWE.

## A. Results for LHC operating at 13 or 14 TeV

## A.1. Parametrization of 13 and 14 TeV cross section as function of the top-quark Yukawa coupling

$$\delta\sigma_{\text{EW}}^{13\text{TeV}}(m_{t\bar{t}} < 2M_t + 50\text{GeV}) = (-0.309 + 0.25g_Y^2)\text{pb}, \tag{28}$$

$$\delta\sigma_{\text{EW}}^{13\text{TeV}}(m_{t\bar{t}} < 2M_t + 50\text{GeV}) = (-0.309 + 0.25g_Y^2)\text{pb}, \qquad (28)$$
  
$$\delta\sigma_{\text{EW}}^{13\text{TeV}}(m_{t\bar{t}} < 2M_t + 100\text{GeV}) = (-0.572 + 0.36g_Y^2)\text{pb}, \qquad (29)$$
  
$$\delta\sigma_{\text{EW}}^{13\text{TeV}}(m_{t\bar{t}} < 2M_t + 150\text{GeV}) = (-0.752 + 0.38g_Y^2)\text{pb}, \qquad (30)$$

$$\delta\sigma_{\text{EW}}^{13\text{TeV}}(m_{t\bar{t}} < 2M_t + 150\text{GeV}) = (-0.752 + 0.38g_Y^2)\text{pb}, \tag{30}$$

$$\delta\sigma_{\text{EW}}^{14\text{TeV}}(m_{t\bar{t}} < 2M_t + 50\text{GeV}) = (-0.360 + 0.29g_Y^2)\text{pb}, \tag{31}$$

$$\delta\sigma_{\text{EW}}^{14\text{TeV}}(m_{t\bar{t}} < 2M_t + 50\text{GeV}) = (-0.360 + 0.29g_Y^2)\text{pb},$$

$$\delta\sigma_{\text{EW}}^{14\text{TeV}}(m_{t\bar{t}} < 2M_t + 100\text{GeV}) = (-0.669 + 0.41g_Y^2)\text{pb},$$

$$\delta\sigma_{\text{EW}}^{14\text{TeV}}(m_{t\bar{t}} < 2M_t + 150\text{GeV}) = (-0.879 + 0.44g_Y^2)\text{pb}.$$
(31)

$$\delta\sigma_{\text{EW}}^{14\text{TeV}}(m_{t\bar{t}} < 2M_t + 150\text{GeV}) = (-0.879 + 0.44g_Y^2)\text{pb}. \tag{33}$$

The relative corrections are given by:

$$\frac{\delta \sigma_{\text{EW}}^{13\text{TeV}}}{\sigma_{\text{LO}}} (m_{t\bar{t}} < 2M_t + 50\text{GeV}) = (-3.753 + 3.08g_Y^2)\%, \tag{34}$$

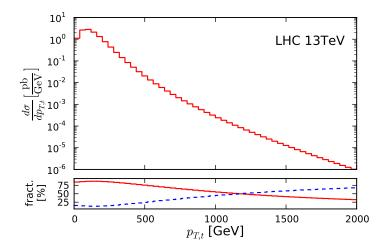


Figure 16: Same as Fig. 6 but for 13 TeV.

$$\frac{\delta \sigma_{\text{EW}}^{13\text{TeV}}}{\sigma_{\text{LO}}} (m_{t\bar{t}} < 2M_t + 100\text{GeV}) = (-3.177 + 1.97g_Y^2)\%, \tag{35}$$

$$\frac{\delta \sigma_{\text{EW}}^{13\text{TeV}}}{\sigma_{\text{LO}}} (m_{t\bar{t}} < 2M_t + 150\text{GeV}) = (-2.908 + 1.45g_Y^2)\%, \tag{36}$$

$$\frac{\delta \sigma_{\text{EW}}^{14\text{TeV}}}{\sigma_{\text{LO}}} (m_{t\bar{t}} < 2M_t + 50\text{GeV}) = (-3.775 + 3.08g_Y^2)\%, \tag{37}$$

$$\frac{\delta \sigma_{\text{EW}}^{14\text{TeV}}}{\sigma_{\text{LO}}} (m_{t\bar{t}} < 2M_t + 100\text{GeV}) = (-3.190 + 1.96g_Y^2)\%, \tag{38}$$

$$\frac{\sigma_{\text{LO}}}{\delta \sigma_{\text{EW}}^{14\text{TeV}}} (m_{t\bar{t}} < 2M_t + 150\text{GeV}) = (-2.914 + 1.44g_Y^2)\%.$$
 (39)

## A.2. Differential distributions for LHC operating at 13 and 14 TeV

## References

- [1] T. Aaltonen *et al.* [CDF and D0 Collaborations], Phys. Rev. D **86** (2012) 092003,
- [2] Tevatron electroweak working group, D0 Note 6363,
- [3] S. Moch and P. Uwer, Phys. Rev. D 78 (2008) 034003,
- [4] M. Aliev, H. Lacker, U. Langenfeld, S. Moch, P. Uwer and M. Wiedermann, Comput. Phys. Commun. **182** (2011) 1034,
- [5] S. Moch, P. Uwer and A. Vogt, Phys. Lett. B **714** (2012) 48,

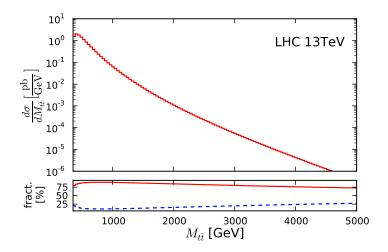


Figure 17: Same as Fig. 7 but for 13 TeV.

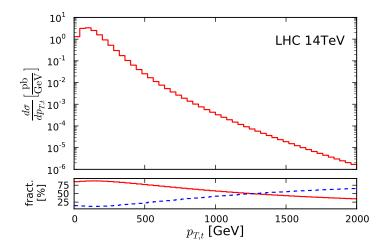


Figure 18: Same as Fig. 6 but for 14 TeV.

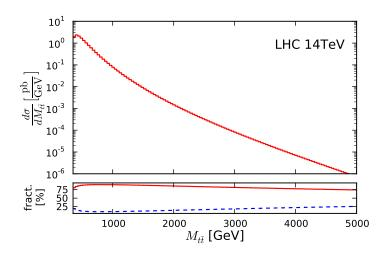


Figure 19: Same as Fig. 7 but for 14 TeV.

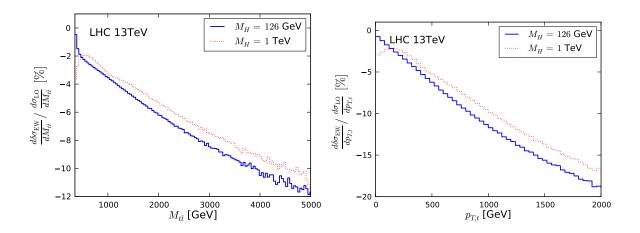


Figure 20: Same as Fig. 12 but for 13 TeV.

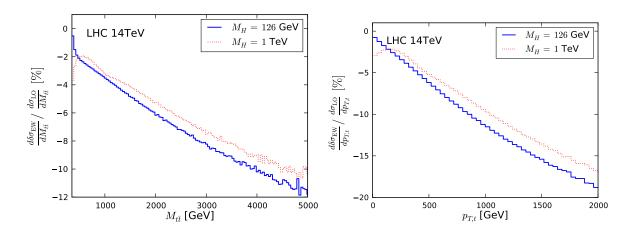


Figure 21: Same as Fig. 12 but for 14 TeV.

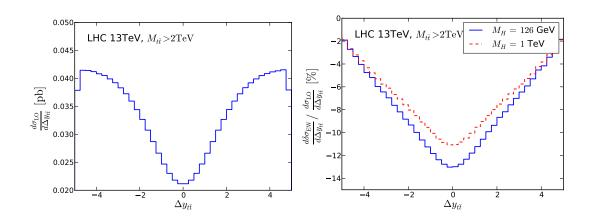


Figure 22: Same as Fig. 13 but for 13 TeV.

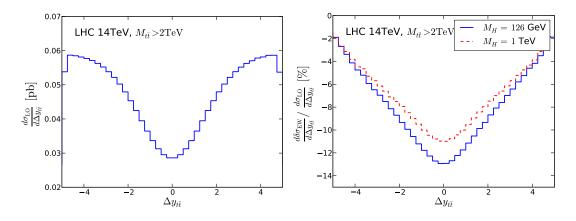


Figure 23: Same as Fig. 13 but for 13 TeV.

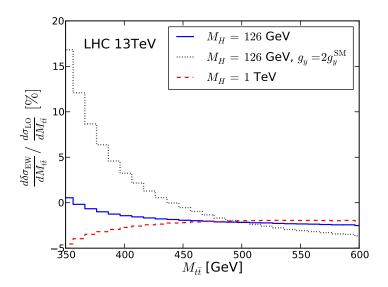


Figure 24: Same as Fig. 14 but for 13 TeV.

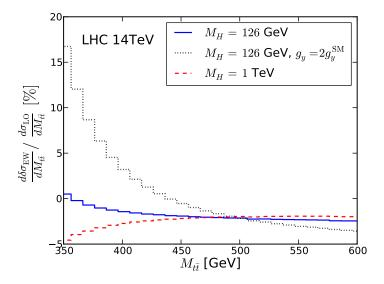


Figure 25: Same as Fig. 14 but for 14 TeV.

- [6] M. Cacciari, M. Czakon, M. Mangano, A. Mitov and P. Nason, Phys. Lett. B 710 (2012) 612,
- [7] P. Baernreuther, M. Czakon and A. Mitov, Phys. Rev. Lett. 109 (2012) 132001,
- [8] M. Czakon and A. Mitov, JHEP 1212 (2012) 054,
- [9] M. Czakon and A. Mitov, JHEP **1301** (2013) 080,
- [10] M. Czakon, P. Fiedler and A. Mitov, Phys. Rev. Lett. 110 (2013) 252004,
- [11] V. Ahrens, A. Ferroglia, M. Neubert, B. D. Pecjak and L. L. Yang, Phys. Lett. B **703** (2011) 135,
- [12] N. Kidonakis and B. D. Pecjak, Eur. Phys. J. C 72 (2012) 2084,
- [13] N. Kidonakis and R. Vogt, Phys. Rev. D **78** (2008) 074005,
- [14] M. Beneke, P. Falgari, S. Klein, J. Piclum, C. Schwinn, M. Ubiali and F. Yan, JHEP **1207** (2012) 194,
- [15] G. Aad et al. [ATLAS Collaboration], Eur. Phys. J. C 73 (2013) 2328,
- [16] G. Aad et al. [ATLAS Collaboration], Phys. Lett. B 717 (2012) 89,
- [17] S. Chatrchyan et al. [CMS Collaboration], Phys. Lett. B 720 (2013) 83,
- [18] S. Chatrchyan et al. [CMS Collaboration], JHEP **1402** (2014) 024,
- [19] V. Khachatryan *et al.* [CMS Collaboration], arXiv:1407.6643 [hep-ex],
- [20] S. Chatrchyan et al. [CMS Collaboration], JHEP 1305 (2013) 065,
- [21] S. Chatrchyan et al. [CMS Collaboration], Eur. Phys. J. C 73 (2013) 2386,
- [22] G. Aad et al. [ATLAS Collaboration], JHEP 1301 (2013) 116,
- [23] S. Chatrchyan *et al.* [CMS Collaboration], Phys. Rev. D **87** (2013) 072002,
- [24] S. Chatrchyan *et al.* [CMS Collaboration], Eur. Phys. J. C **73** (2013) 2339,
- [25] S. Chatrchyan *et al.* [CMS Collaboration], Phys. Rev. D **87** (2013) 072002,
- [26] S. Chatrchyan *et al.* [CMS Collaboration], JHEP **1212** (2012) 015
- [27] G. Aad et al. [ATLAS Collaboration], Phys. Rev. D 88 (2013) 1, 012004,
- [28] V. M. Abazov et al. [D0 Collaboration], Phys. Rev. D 87 (2013) 011103,
- [29] V. M. Abazov et al. [D0 Collaboration], Phys. Rev. D 84 (2011) 112005,
- [30] T. Aaltonen *et al.* [CDF Collaboration], Phys. Rev. D **87** (2013) 092002,
- [31] T. Aaltonen *et al.* [CDF Collaboration], Phys. Rev. D **83** (2011) 112003,

- [32] J. H. Kühn and G. Rodrigo, Phys. Rev. Lett. **81** (1998) 49,
- [33] J. H. Kühn and G. Rodrigo, Phys. Rev. D **59** (1999) 054017,
- [34] L. G. Almeida, G. F. Sterman and W. Vogelsang, Phys. Rev. D 78 (2008) 014008,
- [35] V. Ahrens, A. Ferroglia, M. Neubert, B. D. Pecjak and L. L. Yang, Phys. Rev. D **84** (2011) 074004
- [36] W. Hollik and D. Pagani, Phys. Rev. D 84 (2011) 093003,
- [37] J. H. Kühn and G. Rodrigo, JHEP 1201 (2012) 063,
- [38] W. Bernreuther and Z. -G. Si, Phys. Rev. D 86 (2012) 034026,
- [39] [ATLAS Collaboration], ATLAS-CONF-2012-095,
- [40] [ATLAS and CDF and CMS and D0 Collaborations], arXiv:1403.4427 [hep-ex].
- [41] W. Beenakker, A. Denner, W. Hollik, R. Mertig, T. Sack and D. Wackeroth, Nucl. Phys. B **411** (1994) 343,
- [42] J. H. Kühn, A. Scharf and P. Uwer, Eur. Phys. J. C 45 (2006) 139,
- [43] W. Bernreuther, M. Fuecker and Z. G. Si, Phys. Lett. B 633 (2006) 54,
- [44] W. Bernreuther, M. Fuecker and Z. -G. Si, Phys. Rev. D 74 (2006) 113005,
- [45] J. H. Kühn, A. Scharf and P. Uwer, Eur. Phys. J. C 51 (2007) 37,
- [46] S. Moretti, M. R. Nolten and D. A. Ross, Phys. Lett. B **639** (2006) 513 [Erratum-ibid. B **660** (2008) 607],
- [47] W. Hollik and M. Kollar, Phys. Rev. D 77 (2008) 014008,
- [48] A. D. Martin, W. J. Stirling, R. S. Thorne and G. Watt, Eur. Phys. J. C 63 (2009) 189,
- [49] S. Kretzer, H. L. Lai, F. I. Olness and W. K. Tung, Phys. Rev. D 69 (2004) 114005,
- [50] J. H. Kühn, A. A. Penin and V. A. Smirnov, Eur. Phys. J. C 17 (2000) 97,
- [51] J. H. Kühn, S. Moch, A. A. Penin and V. A. Smirnov, Nucl. Phys. B **616** (2001) 286 [Erratum-ibid. B **648** (2003) 455]
- [52] G. Aad *et al.* [ATLAS Collaboration], Phys. Lett. B **716** (2012) 1,
- [53] S. Chatrchyan et al. [CMS Collaboration], Phys. Lett. B **716** (2012) 30,
- [54] P. Kant, O. M. Kind, T. Kintscher, T. Lohse, T. Martini, S. Mölbitz, P. Rieck and P. Uwer, arXiv:1406.4403 [hep-ph].
- [55] S. Gieseke, T. Kasprzik and J. H. Kühn, arXiv:1401.3964 [hep-ph],
- [56] Y. Kiyo, J. H. Kühn, S. Moch, M. Steinhauser and P. Uwer, Eur. Phys. J. C 60 (2009)

- 375,
- [57] B. Grzadkowski, J. H. Kühn, P. Krawczyk and R. G. Stuart, Nucl. Phys. B **281** (1987) 18,
- [58] M. J. Strassler and M. E. Peskin, Phys. Rev. D 43 (1991) 1500,
- [59] V. S. Fadin and O. I. Yakovlev, Sov. J. Nucl. Phys. **53** (1991) 1053, [Yad. Fiz. **53** (1991) 1721].
- [60] M. Jezabek and J. H. Kühn, Phys. Lett. B 316 (1993) 360,
- [61] R. Harlander, M. Jezabek and J. H. Kühn, Acta Phys. Polon. B 27 (1996) 1781,
- [62] A. Denner, R. J. Guth and J. H. Kuhn, Nucl. Phys. B 377 (1992) 3,
- [63] R. J. Guth and J. H. Kuhn, Nucl. Phys. B 368 (1992) 38,
- [64] F. Caola and K. Melnikov, Phys. Rev. D 88 (2013) 054024,
- [65] N. Kauer and G. Passarino, JHEP 1208 (2012) 116,
- [66] V. Khachatryan et al. [CMS Collaboration], Phys. Lett. B 736 (2014) 64,
- [67] The ATLAS collaboration, ATLAS-CONF-2014-042.